

## Synthesis and characterization of ultrathin metal coordination Prussian blue nanoribbonst

Cite this: *Dalton Trans.*, 2013, **42**, 5242Received 8th January 2013,  
Accepted 18th February 2013

DOI: 10.1039/c3dt00060e

www.rsc.org/dalton

Suping Bao,<sup>a</sup> Wangping Qin,<sup>a</sup> Qihua Wu,<sup>a</sup> Guodong Liang,<sup>\*a,b</sup> Fangming Zhu<sup>a,b</sup> and Qing Wu<sup>a,b</sup>

Ultrathin metal coordination Prussian blue (PB) nanoribbons with tunable width have been successfully synthesized. The morphology and microstructure of PB nanoribbons are characterized using UV-vis, FT-IR, AFM, TEM and XRD. PB nanoribbons synthesized possess an ultrathin thickness of approximately 1 nm and narrow width. The width of PB ribbons can be tuned by varying the chain length of polymeric precursors. The PB hybrid nanoribbons synthesized exhibit enhanced thermal stability and electrochemical activity. The merit of narrow and tunable width as well as ultrathin thickness of PB hybrid nanoribbons along with enhanced thermal stability and electrochemical activity makes them potentially useful in nano-devices, biosensors and so on.

## Introduction

Intense endeavors have been devoted to the construction of metal coordination nanomaterials with varied morphologies due to their versatile properties including reversible redox activity, superior thermal stability, excellent mechanical strength and so on, which give rise to a wide range of potential applications in nano-devices.<sup>1,2</sup> Since Mann and coworkers synthesized metal coordination nanocubes of Prussian blue (PB) in reverse microemulsions,<sup>3</sup> numerous approaches have been developed to regulate the morphology of PB. Talham and coworkers have synthesized two-dimensional PB grids through metal coordination of an amphiphilic pentacyanoferrate complex at the air–water interface.<sup>4</sup> MacLachlan and coworkers have prepared PB nanoworms and nanocontainers by means of self organization of the ferrate-containing diblock copolymers.<sup>5</sup> Mini-emulsion droplets have also been used to

synthesize hollow nanoparticles of PB.<sup>6</sup> More recently, PB nanoparticles with tunable sizes have been synthesized in the presence of polymeric templates.<sup>7,8</sup> However, the synthesis of highly anisotropic PB nanomaterials has been rarely reported.<sup>4</sup>

Nanoribbons featuring narrow and straight-edged stripes represent promising building blocks or connecting units for applications in nano-devices due to their intriguing structure-related physical properties.<sup>9</sup> Although nanoribbons of a number of inorganic or organic materials have been synthesized, including graphene nanoribbons prepared by exfoliating graphite,<sup>9a</sup> unzipping of carbon nanotubes<sup>9b</sup> or chemical vapor deposition processes,<sup>9c</sup> metal oxide or sulfide nanoribbons by thermal evaporation and condensation processes,<sup>9d</sup> dithiopyrene nanoribbons by solution processes *etc.*,<sup>9e</sup> the preparation of nanoribbons with narrow width (<10 nm), in which quantum confinement and the edge effect are significant, remains challenging.<sup>9f</sup> Polypeptides, as one of the most important components of proteins, are able to arrange into  $\alpha$  helix and  $\beta$  fold structures due to supramolecular interaction among amino acid units.<sup>10</sup> Such highly anisotropic structures offer a new opportunity for the achievement of nanoparticles with unique architectures. Herein, we report the synthesis of PB hybrid nanoribbons with ultrathin thickness and tunable width using a cyanoferrate modified polypeptide as the precursor. We demonstrate that the PB hybrid nanoribbons exhibit enhanced thermal stability and electrochemical activity.

## Results and discussion

## Synthesis of PB hybrid nanoribbons

To synthesize PB hybrid nanoribbons, a 4-armed star poly( $\gamma$ -benzyl-L-glutamate) modified with  $\text{NH}_4\text{Na}_2[\text{Fe}(\text{II})(\text{CN})_5-(4-(\text{aminomethyl})\text{pyridine})]$  (PBLG-Fe, **6**) was used (synthesis, ESI†). In a typical experiment, 50 mg PBLG-Fe was suspended in 10 mL distilled water with the assistance of sonication to get a light green suspension. Upon addition of  $\text{Fe}^{3+}$  aqueous solution, the color of the suspension changed to light blue in a few minutes, suggesting the formation of PB. The color

<sup>a</sup>DSAPM Lab, Institute of Polymer Science, School of Chemistry and Chemical Engineering, Sun Yat-Sen University, Guangzhou 510275, P. R. China.

E-mail: lgdong@mail.sysu.edu.cn; Tel: +86-20-84114033

<sup>b</sup>PCFM Lab, OFCM Institute, Sun Yat-Sen University, Guangzhou, 510275, P. R. China

†Electronic supplementary information (ESI) available: AFM height images of PB hybrid nanoribbons and synthesis of PBLG-Fe. See DOI: 10.1039/c3dt00060e

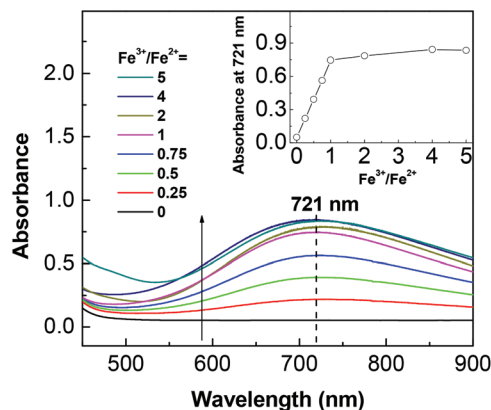


Fig. 1 UV-vis spectra of PBLG-Fe aqueous solution with various amounts of  $\text{Fe}^{3+}$ . The concentration of PBLG-Fe was  $0.30 \text{ mg mL}^{-1}$ .

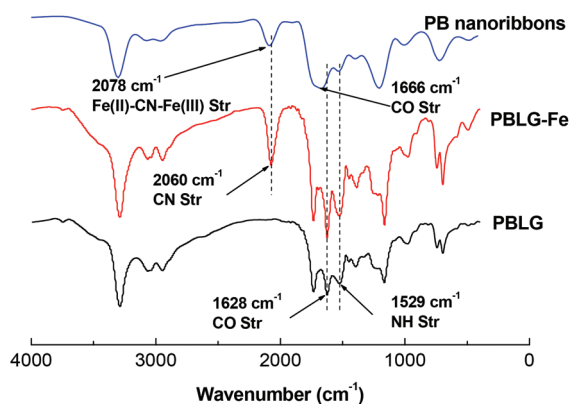


Fig. 2 FT-IR spectra for PBLG, PBLG-Fe and PB hybrid nanoribbons.

change implies that the cyanoferrate complex is accessible to  $\text{Fe}^{3+}$  and is located on the surface of the PBLG-Fe assembly, which enables the subsequent coordination with  $\text{Fe}^{3+}$ . UV-vis results revealed that addition of  $\text{Fe}^{3+}$  led to the appearance of the absorbance band at 721 nm (Fig. 1), attributed to charge transfer of  $\text{Fe(II)-CN-Fe(III)}$ .<sup>11</sup> The intensity of the absorbance band increased with increasing  $\text{Fe}^{3+}$  amounts until molar equivalent  $\text{Fe}^{3+}$  was added, illustrating that  $\text{Fe}^{3+}$  is involved in the coordination polymerization reaction. The FT-IR spectrum of PBLG-Fe showed an absorbance band at  $2060 \text{ cm}^{-1}$  attributable to the  $\text{C}\equiv\text{N}$  stretching vibration (Fig. 2). This band shifted to  $2078 \text{ cm}^{-1}$  after coordination polymerization due to the formation of the  $\text{Fe(II)-CN-Fe(III)}$  bridge.<sup>12</sup>

### Morphology of PB hybrid nanoribbons

The morphology of PB hybrid nanoribbons fabricated was characterized using tapping mode atomic force microscopy (AFM) and transmission electron microscopy (TEM). A typical AFM image revealing ribbon-like structures is shown in Fig. 3. Cross-sectional analysis illustrated that the thickness of PB hybrid nanoribbons was *ca.* 1 nm and the width was 9.7 nm (Fig. S1, ESI†). The thickness of PB hybrid nanoribbons was similar to that of a single PBLG layer sandwiched between two

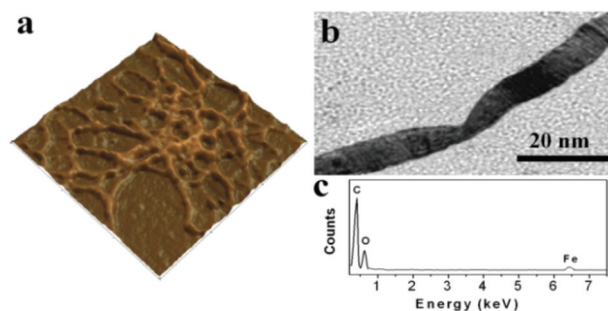


Fig. 3 Tapping mode AFM image (a) with a size of  $600 \text{ nm} \times 600 \text{ nm}$ , TEM image (b) of PB hybrid nanoribbons and EDX spectrum (c).

Prussian blue monolayers. PBLG-Fe is amphiphilic. When PBLG-Fe self organizes in aqueous media, hydrophobic PBLG layers are sandwiched between two hydrophilic ferrate layers. Subsequent coordination polymerization of the cyanoferrate complex with  $\text{Fe}^{3+}$  leads to the formation of tri-layered structures consisting of a PBLG layer sandwiched between two PB monolayers. Moreover, the width of PB hybrid nanoribbons was close to the chain length of fully extended PBLG-Fe macromolecules, implying that PBLG macromolecules aligned perpendicular to the long axes of the ribbons. A typical TEM image of PB hybrid nanoribbons with widths of *ca.* 10 nm is shown in Fig. 3. Some sets of parallel lines with the interline distance of *ca.* 0.5 nm aligned perpendicular to the long axis of the ribbons were discerned in TEM images. The endeavor to obtain EDX elemental mapping was unsuccessful due to rapid degradation of nanoribbons upon exposure to intense electron beams, likely associated with the ultrathin thickness. EDX analysis confirmed the presence of iron in PB hybrid nanoribbons.

### Microstructure of PB hybrid nanoribbons

Polypeptides such as PBLG exhibit secondary structures induced by intramolecular and intermolecular hydrogen bonding in bulk or in solution.<sup>10</sup> The secondary structure of PBLG depending on its molar mass can be verified using FT-IR. The FT-IR spectrum of PBLG showed two distinct absorbance bands at  $1628 \text{ cm}^{-1}$  and  $1529 \text{ cm}^{-1}$  (Fig. 2), being characteristic of  $\beta$  sheets with anti-parallel configuration, ascribed to the  $\text{C}=\text{O}$  and  $\text{C}-\text{N}$  stretching vibrations, respectively.<sup>10a</sup> These bands remained for PBLG-Fe and PB hybrid nanoribbons, demonstrating that inclusion of the ferrate complex and formation of PB did not change the secondary structure of the  $\beta$  sheets of PBLG.

The microstructure of PBLG, PBLG-Fe and PB hybrid nanoribbons was characterized by means of wide-angle X-ray diffraction (XRD), as shown in Fig. 4. Two distinct reflections at  $2\theta = 5.4^\circ$  and  $2\theta = 18.7^\circ$ , attributed to lamellar stacking of  $\beta$  sheets<sup>7a</sup> and the intermolecular distance between adjacent macromolecules within individual  $\beta$  sheets,<sup>7d</sup> respectively, were observed for PBLG. The reflection peak at  $2\theta = 5.4^\circ$  ( $d = 1.61 \text{ nm}$ ) for PBLG shifted to a lower angle  $2\theta = 5.3^\circ$  ( $d = 1.67 \text{ nm}$ ) for PBLG-Fe, revealing that substitution of the benzyl

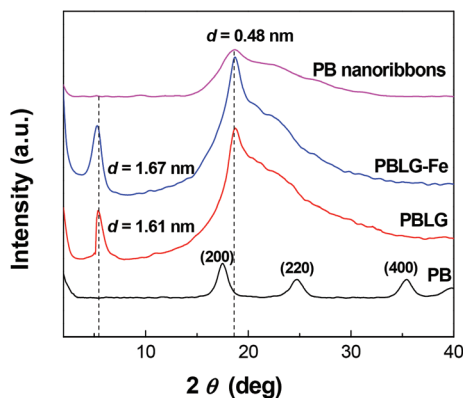


**Fig. 4** X-ray diffraction (XRD) curves of conventional PB, PBLG, PBLG-Fe and PB hybrid nanoribbons.

ester moiety with the bulky ferrate complex enlarged slightly the gallery distance of the  $\beta$  sheets of PBLG. In contrast, this peak disappeared completely for PB hybrid nanoribbons, illustrating irreversible delamination of stacked  $\beta$  sheets. This result was in good agreement with the morphological analysis. Moreover, the diffraction peak at  $2\theta = 18.7^\circ$  ( $d = 0.48$  nm) remained for PBLG-Fe and PB hybrid nanoribbons, indicating that the intermolecular arrangement of PBLG (individual  $\beta$  sheets) was retained. A broad “amorphous halo” at  $2\theta = \sim 23^\circ$  was observed for all samples investigated, derived mainly from the long amorphous side-chains. Moreover, it was worth noting that no reflection peaks from PB crystals were detected for PB hybrid nanoribbons, which implied that PB nanolayers in ribbons were amorphous, likely due to the ultrathin thickness of PB nanolayers.

### Understanding the formation of PB hybrid nanoribbons

PBLG-Fe before sonication consisted of stacked  $\beta$  sheets, as revealed by FT-IR and XRD results. PBLG-Fe can not be dispersed in water even with vigorous stirring. When a PBLG-Fe aqueous mixture was subjected to sonication for 10 min, PBLG-Fe aggregates disappeared and a homogeneous clear solution was obtained. The morphology of PBLG-Fe after sonication was examined using TEM (Fig. S2, ESI<sup>†</sup>). Ribbon-like structures, rather than stacked sheets or lamellae, were observed. This showed that the stacked  $\beta$  sheets of PBLG-Fe were delaminated into ribbon-like structures during sonication of the PBLG-Fe aqueous suspension. Hydrophobic pristine PBLG was unable to disperse in water even using high-power sonication for long durations. Consequently, incorporation of the ferrate complex into PBLG-Fe was crucial for the delamination of stacked  $\beta$  sheets of PBLG and the resulting formation of nanoribbons. Two possible reasons account for the ferrate-incorporation induced delamination of PBLG-Fe: (1) inclusion of the bulky cyanoferrate complex enlarges the gallery distance of the  $\beta$  sheets of PBLG-Fe, as verified by XRD measurement (Fig. 4); (2) electrostatic repulsion among the negatively-charged ferrate complex ions of the  $\beta$  sheets is helpful for the

delamination of stacked  $\beta$  sheets and the formation of nanoribbons.

The PBLG-Fe aqueous suspension after sonication was not stable, and flocculation occurred if left to stand over 30 min. After coordination polymerization with  $\text{Fe}^{3+}$  and forming PB hybrid nanoribbons, the suspension was stable over 3 days, revealing that the formation of PB layers improved the dispersion of hybrid ribbons in aqueous media.

### Tuning width of PB hybrid nanoribbons

PB hybrid nanoribbons consisted of PBLG-Fe macromolecules aligned perpendicular to the long axes, as implied by morphological analysis. This means that the width of the nanoribbons is related to the chain length of PBLG-Fe, and the shorter chain length of PBLG-Fe must lead to narrower nanoribbons. This finding encouraged us to regulate the width of PB hybrid nanoribbons by varying the chain length of the PBLG-Fe, which can be readily achieved by varying the monomer/initiator ratio in the PBLG synthesis process.

We next synthesized PB hybrid nanoribbons with narrower width using PBLG-S-Fe with a decreased molar mass of  $5.8 \text{ kg mol}^{-1}$  (synthesis, ESI<sup>†</sup>). The typical AFM image and cross-sectional profile of nanoribbons (Fig. S3, ESI<sup>†</sup>) showed that PB hybrid nanoribbons had a similar thickness of 1 nm and a decreased width of 6.1 nm, as expected.

### Thermal property of PB hybrid nanoribbons

The thermal stability of PB hybrid nanoribbons was evaluated using thermogravimetric analysis (TGA) (Fig. 5). PBLG began to decompose mainly at  $250^\circ\text{C}$  with a maximum decomposition rate at  $280^\circ\text{C}$ . Decomposition of PBLG almost ceased above  $500^\circ\text{C}$  and PBLG lost 88% of its initial mass. However, PB hybrid nanoribbons only lost 20% of their initial mass even at high temperature ( $500^\circ\text{C}$ ), which indicated that PB hybrid nanoribbons possessed significantly enhanced thermal stability in contrast to PBLG. The possible reason is that sandwiching of PBLG layers between inorganic PB nanolayers restricts the mobility of PBLG macromolecules, which prevents radical species produced during thermal decomposition from

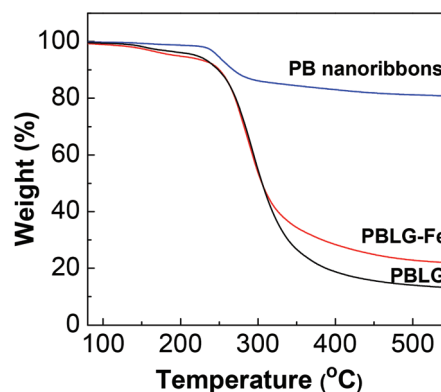


**Fig. 5** Thermogravimetric analysis traces of PBLG, PBLG-Fe and PB hybrid nanoribbons under  $\text{N}_2$ .

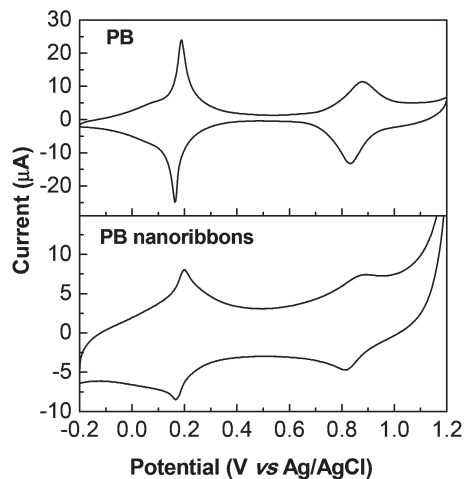


**Fig. 6** Cyclic voltammogram of PB hybrid nanoribbons and conventional PB particles deposited on glassy carbon electrodes. In 0.1 M KCl solution, scan rate: 50 mV min<sup>-1</sup>, under N<sub>2</sub>.

propagating. Moreover, thermal insulating PB nanolayers are inclined to inhibit heat flow during degradation.

#### Electrochemical behavior of PB hybrid nanoribbons

The electrochemical behavior of PB hybrid nanoribbons was measured by using cyclic voltammograms (CVs). A typical CV curve of conventional PB particles showed two sets of distinct redox pairs, located at  $E_{1/2} = 0.18$  V with a peak separation of 25 mV and at  $E_{1/2} = 0.86$  V with a peak separation of 45 mV (Fig. 6), ascribed to reversible Prussian white/Prussian blue and Berlin green (or Prussian yellow)/Prussian blue conversion, respectively.<sup>13</sup> Both the former and the latter redox pairs with peak separations of 33 mV and 56 mV, respectively, were observed for PB hybrid nanoribbons, demonstrating regular PB structures with homogeneous charge distribution through PB layers. The redox peak separations of PB hybrid nanoribbons, associated with the diffusion rates of redox species to the electrode, were comparable to those of three-dimensional (3D) PB particles. This revealed that PB hybrid nanoribbons possessed similar charge diffusion rates to 3D PB particles, despite the amorphous nature of PB layers and the low fraction of PB in hybrid ribbons.

#### Conclusions

In summary, metal coordination Prussian blue (PB) nanoribbons with ultrathin thickness and tunable width were synthesized for the first time. PB hybrid nanoribbons consisted of a single PBLG layer with macromolecules aligned perpendicular to the long axes of ribbons, sandwiched between two amorphous PB nanolayers. TGA results illustrated that PB hybrid nanoribbons exhibited enhanced thermal stability. CV results revealed that PB hybrid nanoribbons were electrochemically active. The intriguing microstructure of PB hybrid

nanoribbons together with their structure-related enhanced properties made them useful in nano-devices, biosensors and so on.

## Experimental section

### Synthesis of PB hybrid nanoribbons

To synthesize PB hybrid nanoribbons, 50 mg PBLG-Fe (synthesis, ESI<sup>†</sup>) was suspended in 10 mL distilled water with the assistance of sonication. To the PBLG-Fe suspension was added a 2 molar equivalent Fe(NO<sub>3</sub>)<sub>3</sub> aqueous solution. The mixture was stirred for 12 h at room temperature. The resulting solution was added dropwise to 100 mL cold methanol with stirring. The mixture was centrifuged and the top layer was decanted. The solid was rinsed with methanol (50 mL × 3) and dried in a vacuum at 40 °C overnight to give light blue powders.

### Characterization

A field emission gun TEM microscope (JEM2010HR) equipped with an Oxford Instrument UTW ISIS EDX system was used to characterize the microstructure of PB hybrid nanoribbons. The acceleration voltage was 200 kV. The sample was prepared by drying a drop of PB hybrid nanoribbon/water suspension on a carbon-coated copper grid. The specimen was directly observed without staining due to the presence of iron. Tapping mode AFM to investigate the three-dimensional morphology of PB nanoribbons was performed using a commercial atomic force microscope (SPM-9500J3) with a silicon micro-cantilever (spring constant 30 N m<sup>-1</sup> and resonance frequency ~270 kHz). The scan rate varied from 0.1 to 2.0 Hz to optimize the image quality. X-ray diffraction (XRD) measurements were performed using an XRD diffractometer (D-MAX 2200 VPC) equipped with Ni-filtered Cu K $\alpha$  radiation, having a wavelength of 0.154 nm. The diffractometer was scanned in  $2\theta$  range from 1.5° to 50° and the scan rate used was 1.2° min<sup>-1</sup>. The TGA curves were recorded using a NetzschTG-209 thermo-balance in a temperature range from 25 to 550 °C at a heating rate of 10 °C min<sup>-1</sup> under nitrogen. UV-vis spectroscopy data were obtained by using a Hitachi U3500 at room temperature. FT-IR spectra were recorded using a Nicolet/Nexus 670 FT-IR spectrophotometer. Powder samples were mixed with KBr and then pressed into pellets for FT-IR measurements. Cyclic voltammetry was performed using a CHI-660D electrochemical analyzer (CH Instruments, Inc.) in a three electrode cell. Glassy carbon working electrodes with a diameter of 3 mm were polished with a slurry of 0.05 µm alumina particles, sonicated and rinsed with ultrapure water. After drying under N<sub>2</sub>, the glassy carbon working electrodes were made hydrophilic by treating in oxygen plasma (1 Torr O<sub>2</sub>, 10 W) for 5 min. The cleaning process was repeated until no voltammetric features were observed in the range from -0.2 to 1.2 V (vs. Ag/AgCl) at the scan rate of 100 mV s<sup>-1</sup> in 0.1 M KCl solution. PB hybrid nanoribbons/water suspension was deposited on freshly cleaned glassy carbon working electrodes. The solvent was

allowed to evaporate at room temperature overnight. 0.1 M KCl solution was used as a buffer solution. To remove oxygen, the buffer solution was degassed by bubbling N<sub>2</sub> for 40 min prior to CV measurements. Every sample was tested three times to obtain reproducible results.

## Acknowledgements

Financial support in part from NSFC (21074151), the Guangzhou Planning Project of Science and Technology (11C52050729), the One Hundred Talents Project of Sun Yat-Sen University, the SRF for ROCS and SEM, and the Hong Kong Scholar Program (XJ2011047) is gratefully acknowledged.

## Notes and references

- 1 P. A. Rugar, L. Chabanne, M. A. Winnik and I. Manners, *Science*, 2012, **337**, 559–562.
- 2 (a) F. H. Schacher, P. A. Rugar and I. Manners, *Angew. Chem., Int. Ed.*, 2012, **51**, 7898–7921; (b) R. Ahmed, A. Priimagi, C. F. J. Faul and I. Manners, *Adv. Mater.*, 2012, **24**, 926–931; (c) J. B. Gilroy, S. K. Patra, J. M. Mitchels, M. A. Winnik and I. Manners, *Angew. Chem., Int. Ed.*, 2011, **50**, 5851–5855.
- 3 (a) S. Vaucher, M. Li and S. Mann, *Angew. Chem., Int. Ed.*, 2000, **39**, 1793–1796; (b) S. Vaucher, J. Fielden, M. Li, E. Dujardin and S. Mann, *Nano Lett.*, 2002, **2**, 225–229.
- 4 J. T. Culp, J. H. Park, D. Stratakis, M. W. Meisel and D. R. Talham, *J. Am. Chem. Soc.*, 2002, **124**, 10083–10090.
- 5 (a) X. Roy, J. K. H. Hui, M. Rabnawaz, G. J. Liu and M. J. MacLachlan, *J. Am. Chem. Soc.*, 2011, **133**, 8420–8423; (b) X. Roy, J. K. H. Hui, M. Rabnawaz, G. J. Liu and M. J. MacLachlan, *Angew. Chem., Int. Ed.*, 2011, **50**, 1597–1602.
- 6 (a) R. McHale, N. Ghasdian, Y. B. Liu, M. B. Ward, N. S. Hondow, H. H. Wang, Y. Q. Miao, R. Brydson and X. S. Wang, *Chem. Commun.*, 2010, **46**, 4574–4576; (b) S. J. Ye, Y. B. Liu, S. J. Chen, S. Liang, R. McHale, N. Ghasdian, Y. Lu and X. S. Wang, *Chem. Commun.*, 2011, **47**, 6831–6833; (c) G. D. Liang, J. T. Xu and X. S. Wang, *J. Am. Chem. Soc.*, 2009, **131**, 5378–5379; (d) Y. B. Liu and X. S. Wang, *Polym. Chem.*, 2012, **3**, 2632–2639.
- 7 (a) H. Ming, N. L. K. Torad, Y. D. Chiang, K. C. W. Wu and Y. Yamauchi, *CrystEngComm*, 2012, **14**, 3387–3396; (b) M. Hu, S. Furukawa, R. Ohtani, H. Sukegawa, Y. Nemoto, J. Reboul, S. Kitagawa and Y. Yamauchi, *Angew. Chem., Int. Ed.*, 2012, **51**, 984–988; (c) N. L. Torad, M. Hu, M. Imura, M. Naito and Y. Yamauchi, *J. Mater. Chem.*, 2012, **22**, 18261–18267; (d) M. Hu and Y. Yamauchi, *Chem. Asian J.*, 2011, **6**, 2282–2286; (e) M. Hu, A. A. Belik, H. Sukegawa, Y. Nemoto, M. Imura and Y. Yamauchi, *Chem. Asian J.*, 2011, **6**, 3195–3199.
- 8 (a) A. Tokarev, P. Agulhon, J. Long, F. Quignard, M. Robitzer, R. A. S. Ferreira, L. D. Carlos, J. Larionova, C. Guerin and Y. Guari, *J. Mater. Chem.*, 2012, **22**, 20232–20242; (b) B. Folch, J. Larionova, Y. Guari, K. Molvinger, C. Luna, C. Sangregorio, C. Innocenti, A. Caneschi and C. Guerin, *Phys. Chem. Chem. Phys.*, 2010, **12**, 12760–12770.
- 9 (a) X. L. Li, X. R. Wang, L. Zhang, S. W. Lee and H. J. Dai, *Science*, 2008, **319**, 1229–1232; (b) D. V. Kosynkin, A. L. Higginbotham, A. Sinitskii, J. R. Lomeda, A. Dimiev, B. K. Price and J. M. Tour, *Nature*, 2009, **458**, 872–876; (c) W. Liu, B. L. Jackson, J. Zhu, C. Q. Miao, C. H. Chung, Y. J. Park, K. Sun, J. Woo and Y. H. Xie, *ACS Nano*, 2010, **4**, 3927–3932; (d) Y. Jiang, W. J. Zhang, J. S. Jie, X. M. Meng, J. A. Zapien and S. T. Lee, *Adv. Mater.*, 2006, **18**, 1527–1532; (e) W. Jiang, Y. Zhou, H. Geng, S. D. Jiang, S. K. Yan, W. P. Hu, Z. H. Wang, Z. G. Shuai and J. A. Pei, *J. Am. Chem. Soc.*, 2011, **133**, 1–3; (f) J. M. Cai, P. Ruffieux, R. Jaafar, M. Bieri, T. Braun, S. Blankenburg, M. Muoth, A. P. Seitsonen, M. Saleh, X. L. Feng, K. Mullen and R. Fasel, *Nature*, 2010, **466**, 470–473.
- 10 (a) P. Papadopoulos, G. Floudas, H. A. Klok, I. Schnell and T. Pakula, *Biomacromolecules*, 2004, **5**, 81–91; (b) K. T. Kim, C. Park, C. Kim, M. A. Winnik and I. Manners, *Chem. Commun.*, 2006, 1372–1374; (c) K. T. Kim, C. Park, G. W. M. Vandermeulen, D. A. Rider, C. Kim, M. A. Winnik and I. Manners, *Angew. Chem., Int. Ed.*, 2005, **44**, 7964–7968; (d) Y. C. Lin and S. W. Kuo, *J. Polym. Sci., Part A: Polym. Chem.*, 2011, **49**, 2127–2137.
- 11 (a) F. Armand, H. Sakuragi and K. Tokumaru, *New J. Chem.*, 1993, **17**, 351–356; (b) S. H. Toma, J. A. Bonacin, K. Araki and H. E. Toma, *Eur. J. Inorg. Chem.*, 2007, 3356–3364.
- 12 (a) S. F. A. Kettle, E. Diana, E. Boccaleri and P. L. Stanghellini, *Inorg. Chem.*, 2007, **46**, 2409–2416; (b) S. Z. Zhan, D. Guo, X. Y. Zhang, C. X. Du, Y. Zhu and R. N. Yang, *Inorg. Chim. Acta*, 2000, **298**, 57–62.
- 13 A. A. Karyakin, *Electroanalysis*, 2001, **13**, 813–819.